FERMILAB CONF-96/260-E

DØ MEASUREMENTS OF BEAUTY PRODUCTION IN $p\overline{p}$ COLLISIONS AT $\sqrt{s} = 1.8$ TeV

MARC M. BAARMAND
(representing the DØ Collaboration)
Department of Physics,
State University of New York,
Stony Brook, NY 11794-3800, USA

Abstract

We report a number of results on beauty production from the DØ experiment at the Fermilab Tevatron Collider operating at $\sqrt{s} = 1.8$ TeV. Measurements of the $b\overline{b}$ production cross section using single muon, muon plus jet and dimuon plus jet triggers, in the data collected in 1992-93, are presented. A preliminary measurement of the $b\overline{b}$ angular correlations using the dimuon data sample is also presented. We find that the b-quark production cross section for $|y^b| < 1.0$ and $p_T^b > 8$ GeV/c is systematically higher than, although consistent within errors with, the next-to-leading order QCD predictions. A similar comparison with QCD is observed in the $b\overline{b}$ ($\mu\mu$) angular correlations, where the shape of the distribution indicates a sizeable contribution from the next-to-leading order processes.

1 Introduction

The study of b-quark production in high energy hadron collisions provides an effective mechanism to test the predictions of perturbative Quantum Chromodynamics (pQCD). B-meson decays also provide valuable insights on CP violation and physics beyond the Standard Model.

Since its birth in 1973, QCD has evolved into an extensive theoretical apparatus to relate the properties of fundamental quarks and gluons to the observed properties of hadronic interactions. The next-to-leading order (NLO) calculations of inclusive b and differential $b\overline{b}$ production cross section have been available for some time [1,2]. At the Tevatron Collider, the CDF and DØ experiments play a major role in confronting the QCD predictions of $b\overline{b}$ production to experimental data. The measurements from these experiments [4,5], as well as the results from the CERN proton-antiproton collider ($\sqrt{s} = 0.63$ TeV) [3] indicate normalization disagreements at levels that have prompted discussions on the effect and contribution of higher order corrections to the Born cross section, and on the applicability of pQCD in this energy regime. The limitations on the range of applicability of fixed-order QCD calculations come from terms of the form $[\alpha_s(Q)\ ln(Q^2/m^2)]^n$ and $[\alpha_s(Q)\ ln(s/Q^2)]^n$, where Q is the scale parameter, m is the heavy quark mass, s is the partonic center-of-mass energy, and n is the order of the calculation [6]. These terms become large with increasing n if either $Q^2/m^2 \gg 1$ or $s/Q^2 \gg 1$, which may already be the case at Tevatron and almost certainly at LHC. Thus, the truncated perturbative calculation may have large scale-dependence and be a poor approximation of the cross section. The Tevatron data allow for a careful investigation of this problem.

It is clear that a successful determination of the b-quark production cross section at Tevatron is crucial in obtaining a reliable extrapolation towards the LHC energy. Other motivations for studying beauty production at Tevatron include: measurement of (running) α_S; probing gluon density at small x; study of gluon fragmentation; heavy quarkonium production; and search for rare B decays (which probes physics beyond the Standard Model).

The Tevatron Collider is a copious source of b-quarks, which can be detected in DØ through semileptonic decays into high p_T (transverse momentum with respect to the beam) non-isolated (accompanied by hadrons from fragmentation and decay) muons. The strong correlation between the b-quark and the decay muon momenta makes it possible to determine the b-quark production cross section using the muon alone, reducing the uncertainties due to the jet reconstruction algorithm and the underlying event activity. The b (B-meson) branching ratios and decay kinematics are well measured from e^+e^- studies, and the momentum smearing due to the B semileptonic decay is partially accounted for by measuring the integrated cross section as a function of p_T.

In our analyses, the b-quark production cross section for $\mid y^b \mid < 1$ is measured from four different processes:

- Inclusive muon: $p\overline{p} \rightarrow b\overline{b}X \rightarrow \mu X$;
- Muon-jets: $p\overline{p} \rightarrow b\overline{b}X \rightarrow \mu + \text{jets}$;
- Dimuon-jets: $p\overline{p} \rightarrow b\overline{b}X \rightarrow \mu\mu + \text{jets}$;
- J/Ψ production: $p\overline{p} \rightarrow b\overline{b}X \rightarrow J/\Psi X \rightarrow \mu\mu X$.

The cross sections derived from the inclusive muon sample [4] and the J/Ψ sample [7] have been published. (For a discussion of the DØ measurements of J/Ψ (quarkonia) production and the small angle b-quark production cross section, see [8].) Only the dimuon-jets sample allows a direct measurement of $b\overline{b}$ correlations, such as the difference in azimuthal angle between the b and $\overline{b}$-quarks, which examines the relative amounts of different b-quark production mechanisms. A relatively large contribution from the NLO gluon splitting processes, which give rise to 3-body topologies, is expected [1].

2 Detector and Event Selection

The DØ detector and trigger system are described in detail elsewhere [9]. DØ, although optimized for studies of high mass and large p_T final states, has large muon detection coverage, thick calorimetry, and good muon trigger and identification, which allow for a viable study of B's in single and dimuon triggers. The central muon system consists of 3 layers of proportional drift tubes and a magnetized iron toroid located between the first two layers. The muon detector provides a measurement of the muon momentum with a resolution parameterized by $\delta(1/p)/(1/p) = 0.18(p-2)/p \oplus 0.008p$, with p in GeV/c. The uranium-liquid argon calorimeter is used to measure both the minimum ionizing energy associated with the muon track and the electromagnetic and hadronic activity associated with heavy quark decay. The total thickness of the calorimeter plus toroid in the central region varies from 13 to 15 interaction lengths which reduces the hadronic punchthrough in the muon system to less than 0.5% of all sources of low transverse momentum muons. The energy resolution for jets is $\approx 80\%/\sqrt{E(\mathrm{GeV})}$.

The data presented here were taken during the 1992-1993 run of the Tevatron collider. A multi-level trigger system was used to define muon triggers. The Level 0 trigger was a scintillation counter array indicating occurance of an inelastic collision. The Level 1 was a hardware trigger which required hits in muon chambers consistent with a beam-produced muon. The Level 2 was a software trigger requiring a reconstructed muon track. In these analyses, the inclusive muon trigger was defined as a Level 1 muon trigger and a good quality Level 2 muon track with $p_T > 3$ GeV/c. Because of high rates, the inclusive muon data sample was taken in dedicated runs. The muon-jets and dimuon-jets samples had the additional trigger requirement of at least one reconstructed jet with transverse energy $E_T > 10$ GeV. The various events were then fully reconstructed offline and subjected to further cuts, which were customized to individual analysis. In general, muons were required to be consistent with the reconstructed event vertex, to have a good match to a central tracking chamber track, and to deposit > 1 GeV of energy in the calorimeter. The cosmic ray background was reduced by requiring muons to have a crossing time in the muon chambers within 100 ns of the beam crossing time. Each muon was also required to have an associated jet with $E_T > 12$ GeV within a cone of $\Delta R = \sqrt{(\Delta\eta)^2 + (\Delta\phi)^2} < 0.8$. In addition, muon candidates in the region $80^\circ < \varphi^\mu < 110^\circ$ were excluded due to poorly measured chamber efficiencies around the Main Ring beam pipe.

For each sample, kinematical and topological requirements were imposed to reduce backgrounds to $b\bar{b}$ production:

- Inclusive muon: Muons with (pseudorapidity) $|\eta^{\mu}| < 0.8$ and $3.5 < p_T^{\mu} < 60.0$ GeV/c. About 16,000 events were selected, corresponding to a total integrated luminosity $\int \mathcal{L}dt = 74$ nb^{-1}.

- Muon-jets: Single muons with $|\eta^{\mu}| < 0.8$ and $p_T^{\mu} > 6$ GeV/c and jets with $E_T > 15$ GeV. About 2700 events were selected, corresponding to a total integrated luminosity $\int \mathcal{L}dt = 228$ nb^{-1}.

- Dimuon-jets: Two muons with $|\eta^{\mu}| < 0.8$, $4 < p_T^{\mu} < 25$ GeV/c and $6 < M^{\mu\mu} < 35$ GeV/c^2. The lower mass limit removed dimuons resulting from the cascade decay of single b-quarks and through J/ψ decays, while the upper limit reduced dimuon decays of the Z boson. An opening angle cut of $\Delta\Phi_{3D} < 165°$ between the muons was also applied to reduce contamination from cosmic ray muons. A total of 397 events passed all selection criteria, corresponding to a total integrated luminosity $\int \mathcal{L}dt = 6.6$ pb^{-1}.

The trigger and offline reconstruction efficiencies were determined by Monte Carlo. ISAJET [10] events were passed through a detailed GEANT [11] simulation of the detector and full trigger simulation and reconstruction programs. Trigger and some offline efficiencies found in this way were cross checked by using appropriate data samples. For the inclusive muon sample, the overall efficiency was estimated to be 10% at 4 GeV/c, rising to a plateau of 28% for $p_T^{\mu} > 6$ GeV/c, whereas for the dimuon sample, the overall efficiency varied as a function of the leading muon (the higher p_T muon) from about 1% at 4 GeV/c to a plateau of 9% at 15 GeV/c.

3 INCLUSIVE MUON AND DIMUON CROSS SECTIONS

The inclusive muon cross section was calculated by correcting the number of measured muons in each p_T bin for the cosmic ray background and dividing by the efficiency, luminosity and the η interval. The differential cross section for $|\eta^{\mu}| < 0.8$ as a function of measured p_T^{μ} is shown in Fig. 1. The data points are shown with the statistical and systematic errors added in quadrature. The systematic errors associated with this measurement included cosmic ray subtraction (5%), luminosity (5%) and muon trigger and offline efficiencies (11%). The curves, calculated using ISAJET and smeared by the muon momentum resolution, show the expected contributions from π/K and W/Z decays, which dominate in $p_T^\mu < 4$ GeV/c and $p_T^\mu > 30$ GeV/c respectively.

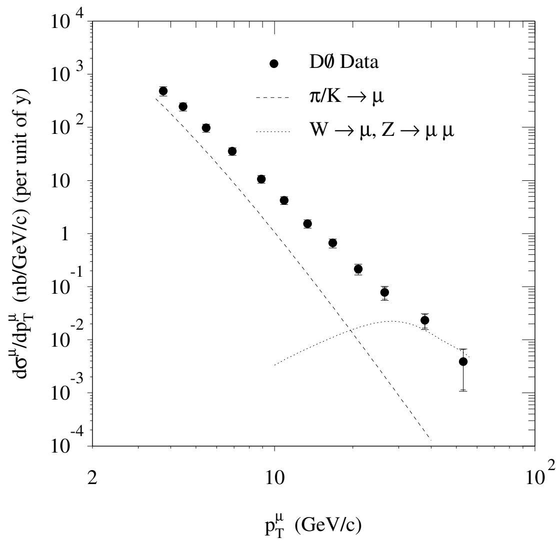

Figure 1: Inclusive muon cross section for $|\eta^\mu| < 0.8$ as a function of measured p_T^μ.

ISAJET was used to extract the fraction of the inclusive muons coming from the b-quark decays. To cross check the ISAJET predictions, we used the quantity p_T^{rel}, which is the transverse momentum of the muon with respect to the associated jet axis (including the muon momentum). For each muon p_T bin, the p_T^{rel} distribution in data was fitted as the sum of the p_T^{rel} distributions from b- and c-quark decays plus π/K decays with the parent distributions given by ISAJET. Good agreement was observed between the ISAJET b-quark fraction and that obtained from the fitting procedure. The systematic uncertainty in the b-quark fraction was estimated to be 13%. Applying the ISAJET b-quark fraction, we obtained the inclusive muon cross section originating from b-quark decays.

Similarly, a muon cross section from the muon-jets data sample was obtained. To calculate the cross section for the dimuon sample, further studies were done. In addition to $b\bar{b}$ production, dimuon events in the mass range 6-35 GeV/c^2 can also arise from $c\bar{c}$ pairs, events in which one or both of the muons are produced by in-flight decays of π or K mesons, Drell-Yan production, Υ decays, and cosmic rays. Muons from Drell-Yan and Υ decays are not expected to have jets associated with them. Monte Carlo estimates normalized to the measured Drell-Yan and Υ cross sections [12] showed that less than one event is expected to contribute to the final data sample from these two sources.

To extract the fraction of the dimuons coming from the b-quark decays, a maximum likelihood fit [13] was used. Four different input distributions were used in the fit: p_T^{rel}, for both the leading and trailing muon, the fraction of longitudinal momentum of the jet carried by the leading muon divided by the jet E_T, z', and the reconstructed time of passage, t_0^f, of the leading muon track through the muon chambers with respect to the beam crossing time. The last variable, t_0^f, was used to subtract the cosmic ray muon background which is not expected to pass in time with the beam crossing.

The p_T^{rel} and z' distributions for $b\overline{b}$, $c\overline{c}$, and b or c plus π/K decay were modeled using the ISAJET Monte Carlo. Each of these samples was processed with a complete detector, trigger, and offline simulation. The distributions for t_0^f were obtained from muons from J/ψ decays and from cosmic ray muons obtained during special runs. Figure 2 shows the result of the maximum likelihood fit for p_T^{rel} of the leading and trailing muons. Also shown are the contributions from the various sources of dimuon events. From the fit, we obtained the number of $b\overline{b}$ events in each bin as a function of p_T^{μ} of the leading muon and as a function of the difference in azimuthal angle between the two muons, $\Delta\phi^{\mu\mu}$. The systematic errors on the number of $b\overline{b}$ events in each bin ($\simeq$ 8%) were estimated by varying the input distributions to the maximum likelihood fit. The fitting results were checked using Monte Carlo dimuon events, where all trigger and offline selection cuts were included. Good agreement between the Monte Carlo and fitting results was observed.

The dimuon cross section originating from $b\overline{b}$ production was calculated using

$$\frac{d\sigma_{b\overline{b}}^{\mu\mu}}{dp_T^{\mu_1}} = \frac{1}{\Delta p_T^{\mu_1}} \frac{N_{b\overline{b}} f_p}{\epsilon \int \mathcal{L} dt} \tag{1}$$

and

$$\frac{d\sigma_{b\overline{b}}^{\mu\mu}}{d\Delta\phi^{\mu\mu}} = \frac{1}{\Delta\phi^{\mu\mu}} \frac{N_{b\overline{b}} f_p}{\epsilon \int \mathcal{L} dt}, \tag{2}$$

where μ_1 refers to the leading muon in the event, and f_p is an unfolding factor to account for the smearing due to the muon momentum resolution. An unfolding technique [14] was used to determine f_p. f_p varies from ≈ 0.78 at low $p_T^{\mu_1}$ to ≈ 0.93 in the highest $p_T^{\mu_1}$ bin. The systematic uncertainty associated with f_p was estimated to be 43% in the low $p_T^{\mu_1}$ bin to $\approx$ 5% in the highest $p_T^{\mu_1}$ bin. The total systematic error was found to be $p_T^{\mu_1}$ dependent, ranging from 18-48%. It included uncertainties from trigger efficiency (19%), offline selection cuts (5%), likelihood fit (6%), and the integrated luminosity (5%).

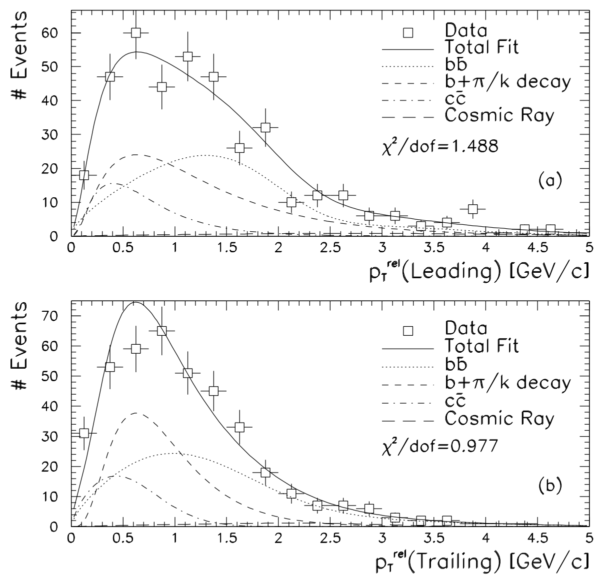

Figure 2: The results of the maximum likelihood fit to the data for (a) p_T^{rel} of the leading muon and (b) p_T^{rel} of the trailing muon. Also shown are the contributions from various dimuon processes.

4 b-QUARK CROSS SECTION

To extract the b-quark cross section, we employed a method first used by UA1 [3]. Since a correlation exists between the p_T of the muons produced from b-quark decays and the parent b-quark p_T, the muon p_T cuts in the data are effectively b-quark p_T cuts. For a set of kinematic cuts, we define p_T^{min} as that value of the b-quark p_T such that 90% of the accepted events have b-quark transverse momentum greater than p_T^{min}. The b-quark cross section, for example from the dimuons, can then be calculated as

$$\sigma_b(p_T^b > p_T^{min}) = \sigma_{b\bar{b}}^{\mu\mu}(p_T^{\mu_1})\frac{\sigma_b^{MC}}{\sigma_{b\bar{b}\to\mu\mu}^{MC}}, \tag{3}$$

where $\sigma_{b\bar{b}}^{\mu\mu}(p_T^{\mu_1})$ is the measured dimuon cross section of Eq. (1) integrated over different intervals of $p_T^{\mu_1}$, σ_b^{MC} is the total Monte Carlo b-quark cross section for $p_T^b > p_T^{min}$, and $\sigma_{b\bar{b}\to\mu\mu}^{MC}$ is the Monte Carlo cross section for dimuon production with cuts that match the data set. For each interval of $p_T^{\mu_1}$, p_T^{min} is calculated using ISAJET. Similarly, we calculated the b-quark cross section from the inclusive muon and muon-jets samples. Additional uncertainties incurred when extracting the b-quark cross section include B-hadron leptonic branching fraction (7%), parameterization in the fragmentation (20%), and muon decay spectrum (11%).

The results for the b-quark production cross section as a function of p_T^{min}, for $|y^b| < 1.0$, are shown in Fig. 3. Also included are the measurements of the b-quark cross section measured from the J/Ψ sample [7]. The curves represent the NLO QCD predictions [1] using $m_b = 4.75$ GeV/c^2 and the MRSD0 [15] structure functions with $\Lambda^5_{\overline{MS}} = 140$ MeV. The theoretical uncertainty results from varying the QCD mass scale between 100< $\Lambda^5_{\overline{MS}}$ <187 MeV and the factorization and renormalization scale, μ, in the range $\mu_0/2 < \mu < 2\mu_0$, where $\mu_0^2 = m_b^2 + \langle p_T^b \rangle^2$. The various measurements agree rather well with each other but systematically lie above the QCD prediction.

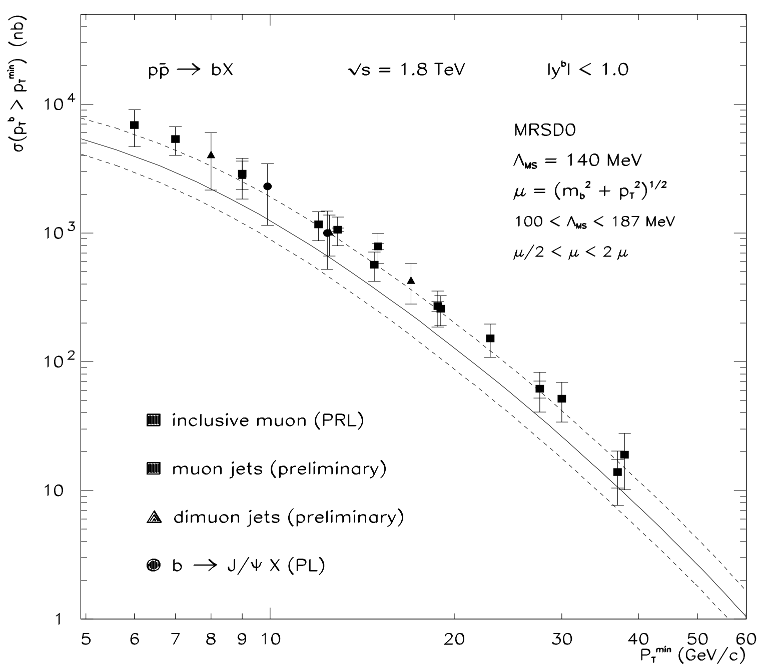

Figure 3: The b-quark production cross section compared with the NLO QCD predictions. The error bars represent the total of statistical and systematic errors.

Figure 4 shows the ratio of the measured and theoretical cross sections as a function of p_T^{min} for DØ and the previous measurements made by UA1 at $\sqrt{s} = 0.63$ TeV [3]. In both cases the predictions underestimate the data, in DØ by a factor of 1.9±0.2.

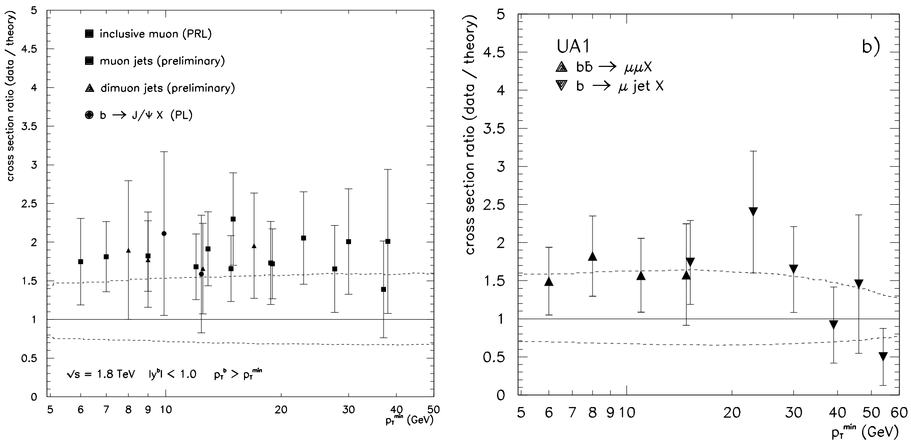

Figure 4: The ratio of the measured and theoretical cross sections as a function of p_T^{min} for DØ and UA1. The dotted curves show the theoretical uncertainties.

5 $b\bar{b}$ Correlations

The differential $b\bar{b}$ cross section calculated in Eq. (2) gives further information on the underlying QCD production mechanisms by studying the topological correlation between the two b-quarks. The difference between the azimuthal angle between the b and $\bar{b}$-quarks (or nearly equivalently, between the decay muons), allows us to differentiate between the contributing QCD production mechanisms, which are the leading order process (flavor creation) and the next-to-leading order processes (gluon splitting, flavor excitation and gluon radiation). There are also contributions from the interference terms. Figure 5 shows the expected $\Delta\phi^{\mu\mu}$ distributions for the different production mechanisms after the dimuon cuts, calculated using the phenomenological model of ISAJET. A sizeable contribution from the higher order processes is expected in the region of $\Delta\phi^{\mu\mu} < 150$ degrees, where the leading order contribution is small.

Figure 6 shows the cross section $d\sigma_{b\bar{b}}^{\mu\mu}/d\Delta\phi^{\mu\mu}$ after acceptance correction for the three-dimensional opening angle cut. The measured $\Delta\phi^{\mu\mu}$ distribution

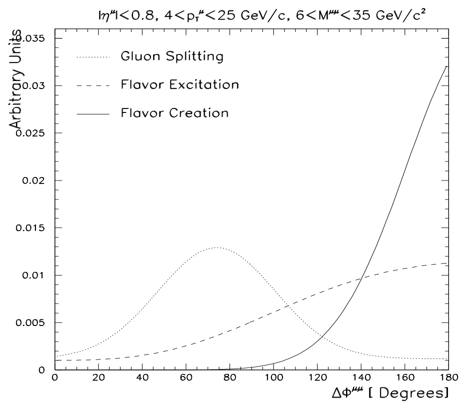

Figure 5: The ISAJET $\Delta\phi^{\mu\mu}$ distributions for the different production mechanisms.

clearly indicates the presence of the higher order processes. It is compared with the NLO QCD prediction determined using the HVQJET [16] Monte Carlo event generator. HVQJET is a direct implementation of the MNR calculation, which is the only fully differential description of the correlated heavy quark production in hadron collisions currently available. HVQJET combines the positive and negative weighted "partonic events", when the event topologies are similar, to cancel the infra-red and collinear divergences in the cross sections. A modified version of ISAJET is then used to do the parton hadronization, particle decays and the interaction of spectator quarks (underlying event). The prediction shown in Fig. 6 includes only gluon-gluon initiated subprocesses but other subprocess contributions are expected to be small.

The data show a clear excess above the HVQJET prediction but agree with the overall shape. The ratio between the data and the $\Delta\phi^{\mu\mu}_{HVQJET}$ is also shown. A zero-order polynomial fit to this ratio indicates that the data differ from the NLO calculation by an overall constant of 1.9$\pm$0.3.

6 Conclusions

In conclusion, several different DØ data sets give consistent measurements of the b-quark production cross section for $|y^b| < 1.0$ in $p\overline{p}$ collisions at $\sqrt{s} = 1.8$ TeV. The measurements are found to agree in shape with the NLO QCD calculation of heavy flavor production, but lie above the central value of the prediction and close to the upper edge of the theoretical uncertainty. Preliminary results on $b\overline{b}$ angular correlations (for $\langle p_T^b \rangle \approx 20$ GeV/c)

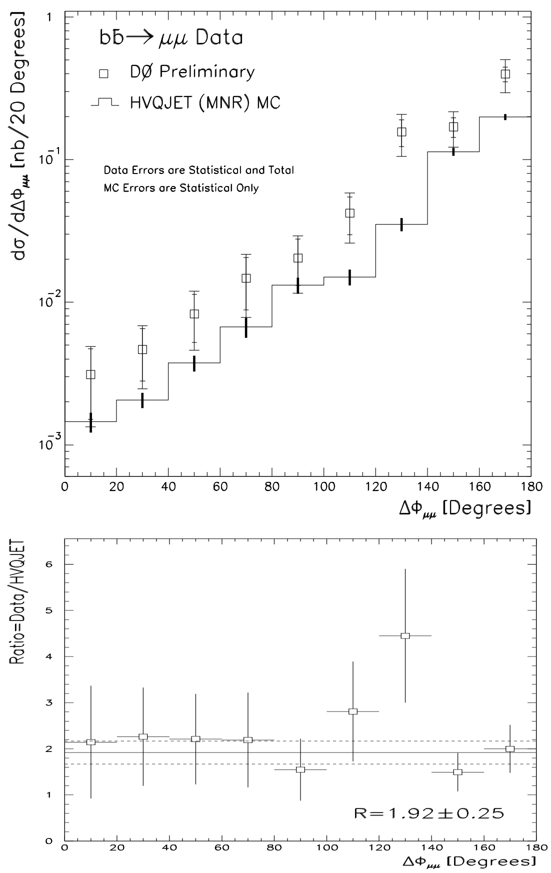

Figure 6: The $\Delta\phi^{\mu\mu}$ spectrum for $b\overline{b}$ production compared to the HVQJET spectrum (see text) and the ratio between the data and HVQJET. The straight line shows the fit to this ratio.

show a similar comparison with QCD: the shape of $d\sigma/d\Delta\phi_{\mu\mu}$ is in agreement with NLO QCD, allowing for a sizeable contribution from higher order processes, and, as expected, the data lie above the prediction by the same factor seen in the inclusive b-quark production cross section.

7 Acknowledgments

We thank the staffs at Fermilab and the collaborating institutions for their contributions to the success of this work, and acknowledge support from the Department of Energy and National Science Foundation (U.S.A.), Commissariat à L'Energie Atomique (France), Ministries for Atomic Energy and Science and Technology Policy (Russia), CNPq (Brazil), Departments of Atomic Energy and Science and Education (India), Colciencias (Colombia), CONACyT (Mexico), Ministry of Education and KOSEF (Korea), CONICET and UBACyT (Argentina), and the A.P. Sloan Foundation.

8 References

1. P. Nason, S. Dawson, and R. K. Ellis, Nucl. Phys. **B303**, 607 (1988); Nucl. Phys. **B327**, 49 (1989).
   W. Beenakker, W. L. van Neerven, R. Meng, G. A. Schuler and J. Smith, Phys. Rev. **D40**, 54 (1989); Nucl. Phys. **B351**, 507 (1991).
2. M. Mangano, P. Nason, and G. Ridolfi, Nucl. Phys. **B373**, 295 (1992).
3. UA1 Collaboration, C. Albajar *et al.*, Phys. Lett. B **256**, 121 (1991); Z. Phys. C **61**, 41 (1994).
4. DØ Collaboration, S. Abachi *et al.*, Phys. Rev. Lett. **74**, 3548 (1995); Phys. Lett. B **370**, 239 (1996).
5. CDF Collaboration, F. Abe *et al.*, Phys. Rev. Lett. **68**, 2403 (1992); **69**, 3704 (1992); **71**, 500 (1993); **71**, 2396 (1993); **71**, 2537 (1993).
6. J. Smith and W. K. Tung, Proceedings of the Workshop on B Physics at Hadron Accelerators, Snowmass, Colorado, June 21- July 2, 1993.
7. DØ Collaboration, S. Abachi *et al.*, Phys. Lett. B **370**, 239 (1996).
8. K. Johns, contribution to these proceedings.
9. DØ Collaboration, S. Abachi *et al.*, Nucl. Instr. Meth. **A338**, 185 (1994).
10. F. Paige and S. Protopopescu, BNL Report No. BNL38034, 1986 (unpublished), release v 7.0.
11. F. Carminati *et al.*, "GEANT Users Guide", v 3.15, CERN Program Library, 1991 (unpublished).
12. A. Smith, Ph.D. Thesis, University of Arizona (1996), unpublished.
13. D. Fein, Ph.D. Thesis, University of Arizona (1996), unpublished.
14. G.D'Agostini, DESY Report No. 94-099, 1994.
15. A. Martin, R. Roberts, and J.W. Sterling, Phys. Rev. D **47**, 867 (1993).
16. M. M. Baarmand, DØ Note 2517, 1995.